Inorganic Chemistry

Article

pubs.acs.org/IC

Enhanced Spin-Crossover Behavior Mediated by Supramolecular Cooperative Interactions

Zheng Yan,[†] Jin-Yan Li,[†] Tao Liu,[‡] Zhao-Ping Ni,*[,†] Yan-Cong Chen,[†] Fu-Sheng Guo,[†] and Ming-Liang Tong*[,†]

[†]Key Laboratory of Bioinorganic and Synthetic Chemistry of Ministry of Education, State Key Laboratory of Optoelectronic Materials and Technologies, School of Chemistry and Chemical Engineering, Sun Yat-Sen University, Guangzhou 510275, P. R. China

[‡]State Key Laboratory of Fine Chemicals, Dalian University of Technology, 2 Linggong Road, Dalian 116024, P. R. China

Supporting Information

ABSTRACT: Three one-dimensional (1D) hetereobimetallic coordination polymers $[Fe^{II}(L)_2(AgCN)_2]\cdot Solv$ (L = bpt^-, **1**; L = $Mebpt^-$, Solv = 1.75EtOH, **2**; L = $bpzt^-$, **3**) with in situ generated AgCN species were synthesized by solvothermal reactions of Fe^{II} salt, $K[Ag(CN)_2]$, and the corresponding ligands [bptH = 3,5-bis(pyridin-2-yl)-1,2,4-triazole, MebptH = 3-(3-methyl-2-pyridyl)-5-(2-pyridyl)-1,2,4-triazole, and bpztH = 3,5-bis(pyrazin-2-yl)-1,2,4-triazole]. They were further characterized by X-ray crystallography, magnetic and photomagnetic measurements, and differential scanning calorimetry. Single-crystal X-ray analyses show that they are isostructural with 1D zigzag chain structures with rhombus $\{Fe_2Ag_2\}$ units, in which the substituted bpt^- ligand connects the Fe^{II} ion and AgCN species in a cis bridging mode. Then the zigzag chains are packed into three-dimensional supramolecular structures by $\pi\cdots\pi$ interactions. Most importantly, weak Ag···N interactions (2.750 Å at 150 K) between the π-stacked neighboring chains present in complex **3**. Magnetic susceptibility measurements exhibit that complex **1** displays characteristic paramagnetic behavior in the temperature range investigated. Complex **2** undergoes a gradual spin-crossover (SCO) with critical temperatures $T_{1/2}\downarrow$ = 232 K and $T_{1/2}\uparrow$ = 235 K, whereas **3** exhibits an abrupt SCO with critical temperatures $T_{1/2}\downarrow$ = 286 K and $T_{1/2}\uparrow$ = 292 K. The magnetostructural relationships suggest that the magnetic behaviors can be modulated from paramagnetic behavior to abrupt and hysteretic SCO near room temperature through adjustment of the electronic substituent effect and intermolecular interactions.

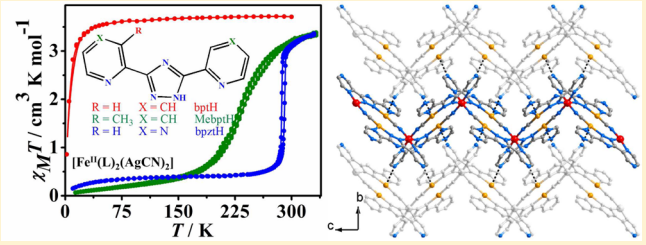

INTRODUCTION

Spin-crossover (SCO), a spin-switching phenomenon that may exist in d^4–d^7 transition metals, has been extensively explored for potential uses in data storage and display devices.[1] For practical applications, abrupt and hysteretic SCO behavior centered near room temperature is usually required,[2] in which dramatic magnetic and physical responses of octahedral $3d^6$ Fe^{II} complexes are associated with the transition between high (HS; $^5T_2$; S = 2) and low (LS; $^1A_1$; S = 0) spin states driven by an external stimulus, i.e., temperature, irradiation, or pressure.[1] However, designing new SCO materials that can meet all of these requirements still remains a challenge.

Iron(II) 1,2,4-triazole is one of famous families to undergo SCO around room temperature with hysteresis,[2a] in which the cooperativity plays a key role in the abruptness and hysteresis. It can be enhanced by covalent bond, hydrogen bonding, $\pi\cdots\pi$ stacking, etc.[3] Then, the substituents at the C^3, N^4, and C^5 positions based around 1,2,4-triazole moieties provide rich and diverse families to explore the impacts of the electronic substituent effect and crystal packing on the SCO properties.[4] Among them, a 2-pyridyl group at the C^3 and C^5 positions of 1,2,4-triazole is capable of forming five-membered chelate rings to construct Fe^{II} complexes. The HS or LS states of two apical Fe^{II} ions coordinated by three chelating ligands in the trigonal-bipyramidal $[\{Fe^{II}(\mu\text{-bpt})_3\}_2Fe^{II}{}_3(\mu_3\text{-O})]^{2+}$ [bptH = 3,5-bis-(pyridin-2-yl)-1,2,4-triazole] cations can be adjusted by different counterions.[5] By using the auxiliary ligands, it can form binuclear Fe^{II} complexes $[\{Fe(NCX)(py)\}_2(\mu\text{-bpt})_2]$ (X = S, Se, BH_3), in which only the stronger field $NCBH_3^-$ ligand displayed a two-step SCO property.[6] By introduction of the $[Au(CN)_2]^-$ unit with the 3-(3-methyl-2-pyridyl)-5-(2-pyridyl)-1,2,4-triazole (MebptH) ligand, one-dimensional (1D) and two-dimensional (2D) SCO supramolecular isomers $[Fe(Mebpt)\{Au(CN)_2\}]_n$ can be obtained.[7] Hence, we initially tried to introduce the $[Ag(CN)_2]^-$ unit with the Fe^{II} ion and bptH ligand to construct a new framework with high dimensionality. However, we obtained the unique 1D coordination polymer $[Fe(bpt)_2(AgCN)_2]$ (**1**) with unexpected in situ generated AgCN species. Unfortunately, the magnetic measurement showed that **1** displayed paramagnetic behavior. Encouraged by the fact that SCO is dramatically affected by the electronic substituent effect and intermolecular interactions,[1,3b] a methyl group and a nitrogen atom were introduced into the pyridine ring in the ligand of **1** (Scheme 1), respectively, resulting in two additional similar 1D hetereobimetallic

Received: May 21, 2014
Published: July 14, 2014

   dx.doi.org/10.1021/ic5011902 | Inorg. Chem. 2014, 53, 8129–8135

Scheme 1. Molecular Structures of the Ligands in 1−3

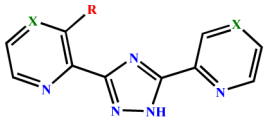

coordination polymers, $[Fe^{II}(Mebpt)_2(AgCN)_2]\cdot 1.75EtOH$ (**2**) and $[Fe^{II}(bpzt)_2(AgCN)_2]$ (**3**). The methyl group at the meta position of pyridine is supposed to increase the ligand field,[8] while the nitrogen atom has an opportunity to increase the intermolecular interactions. As expected, their magnetic behaviors are greatly modulated.

EXPERIMENTAL SECTION

Materials and General Procedures. Three organic ligands and $K[Ag(CN)_2]$ were purcharsed from Jinan Camolai Trading Company. All of the other reagents were obtained commercially and used without further purification. UV−vis spectra were collected by a Cary 5000 UV−vis−near-IR spectrophotometer on the crystal samples of **2** and **3**. IR spectra were collected in KBr tablets in the range 400−4000 cm^{-1} on a Bruker-tensor 27 spectrometer. Elemental analyses (EA) based on the crystal samples were recorded by an Elementar Vario EL elemental analyzer. Differential scanning calorimetry (DSC) measurements were performed by a Netzsch DSC 204 F1 Phoenix instrument under nitrogen with a scan rate of 10 K min^{-1}. Powder X-ray diffraction (PXRD) experiments were performed with a Bruker D8 ADVANCE X-ray diffractometer (Cu Kα = 1.54056 Å). Temperature-dependent magnetic susceptibility data were recorded by a Quantum Design MPMS-XL-7 SQUID magnetometer under a field of 0.1 T. The samples were wrapped with plastic film and mounted in plastic straws. The magnetization of the plastic film and straws was corrected. The diamagnetism correction of **1**−**3** was calculated from Pascal constants. The characterizations of PXRD (Figure S1 in the Supporting Information SI), EA, DSC, and magnetic susceptibility were performed on crystal samples from the same batch.

Synthesis. *$[Fe(bpt)_2(AgCN)_2]_n$ (**1**).* A mixture solution of $FeSO_4\cdot 7H_2O$ (0.028 g, 0.1 mmol), bptH (0.045 g, 0.2 mmol), and $K[Ag(CN)_2]$ (0.040 g, 0.2 mmol) in isopropyl alcohol (7 mL) and cyclohexane (1 mL) was enclosed in a 15 mL Teflon-lined reactor. It was heated at 160 °C for 3 days and cooled slowly (−5 °C h^{-1}) to room temperature. Yellow block crystals were collected in 65% yield. Elem anal. Calcd for **1**: C, 40.66; H, 2.10; N, 21.88. Found: C, 40.71; H, 2.29; N, 21.64. IR (KBr, cm^{-1}): 2158 [s, ν(C≡N)].

*$[Fe(Me\text{-}bpt)_2(AgCN)_2]_n\cdot 1.75nEtOH$ (**2**).* A mixture solution of $FeSO_4\cdot 7H_2O$ (0.028 g, 0.1 mmol), MebptH (0.048 g, 0.2 mmol), and $K[Ag(CN)_2]$ (0.040 g, 0.2 mmol) in ethanol (7 mL) and cyclohexane (1 mL) was enclosed in the reactor, which was heated at 160 °C for 3 days and cooled slowly (−5 °C h^{-1}) to room temperature. Red prism crystals were collected in 37% yield. Elem anal. Calcd for **2**: C, 43.13; H, 3.48; N, 19.22. Found: C, 43.27; H, 3.27; N, 18.92. IR (KBr, cm^{-1}): 2153 [s, ν(C≡N)].

*$[Fe(bpzt)_2(AgCN)_2]_n$ (**3**).* A solution of $Fe(ClO_4)_2\cdot 6H_2O$ (0.036 g, 0.1 mmol), bpztH (0.045 g, 0.2 mmol), and $K[Ag(CN)_2]$ (0.040 g, 0.2 mmol) in ethanol (8 mL) and triethylamine (0.2 mmol) was enclosed in the reactor, which was heated at 160 °C for 3 days and cooled slowly (−5 °C h^{-1}) to room temperature. Red black block crystals were collected in 42% yield. Elem anal. Calcd for **3**: C, 34.23; H, 1.57; N, 29.03. Found: C, 34.07; H, 1.62; N, 29.10. IR (KBr, cm^{-1}): 2145 [s, ν(C≡N)].

X-ray Structure Determination. Diffraction measurements of **1**−**3** were performed with a Bruker SMART Apex CCD diffractometer or a Rigaku R-AXIS SPIDER IP diffractometer (Mo Kα, λ = 0.71073 Å) at various temperatures. These data were solved by direct methods. All non-hydrogen atoms were refined anisotropically by the *SHELXTL* program.[9a] All hydrogen atoms were created by the riding mode. The electron density of disordered ethanol molecules was deleted by the *SQUEEZE* function[9b] in *PLATON* software.[9c] The crystallographic data and refinement parameters are shown in Table 1. CCDC 991150 (**1**_298 K), 991151 (**2**_150 K), 991152 (**2**_298 K), 991153 (**3**_150 K), and 991154 (**3**_298 K) are the supplementary crystallographic data for this paper. They can be obtained freely from the Cambridge Crystallographic Data Center via www.ccdc.cam.ac.uk/data_request/cif.

RESULTS AND DISCUSSION

Synthesis. Complexes $[Fe(L)_2(AgCN)_2]\cdot Solv$ (L = bpt^-, **1**; L = $Mebpt^-$, Solv = $1.75C_2H_5OH$, **2**; L = $bpzt^-$, **3**) were synthesized by solvothermal reactions of Fe^{II} salt, $K[Ag(CN)_2]$, and the corresponding bidentate ligand L in a 1:2:2 ratio at 160 °C for 3 days. Unlike our previous work for $[Fe(Mebpt)\{Au(CN)_2\}]_n$,[7] an unexpected AgCN species was generated, which is likely due to the higher reaction temperature and relatively

Table 1. Crystal Data and Refinement Parameters for 1−3

	1		2		3
Fe^{II} spin state	HS	LS	HS	LS	HS
T [K]	298	150	298	150	298
formula	$C_{26}H_{16}Ag_2FeN_{12}$	$C_{28}H_{20}Ag_2FeN_{12}O_{1.75}$	$C_{28}H_{20}Ag_2FeN_{12}O_{1.75}$	$C_{22}H_{12}Ag_2FeN_{16}$	$C_{22}H_{12}Ag_2FeN_{16}$
fw	768.10	876.77	876.77	772.07	772.07
space group	$C2/c$	$C2/c$	$C2/c$	$P2/c$	$P2/c$
a (Å)	19.4761(13)	20.9431(15)	21.236(2)	9.6911(3)	9.8571(3)
b (Å)	12.4556(9)	13.3205(4)	13.6005(12)	9.0833(3)	9.4122(2)
c (Å)	13.9142(9)	12.8167(9)	12.9411(12)	14.3017(6)	14.2352(5)
β (deg)	124.811(2)	112.733(9)	112.208(2)	103.760(4)	103.610(3)
V (Å)^3	2771.3(3)	3297.7(3)	3460.3(6)	1222.81(8)	1283.61(7)
Z	4	4	4	2	2
D_{calcd} (g cm^{-3})	1.841	1.766	1.683	2.097	1.998
reflns collected	3090	2485	3938	1794	1869
unique reflns	2169	2133	1796	1664	1548
R_{int}	0.0286	0.0277	0.0624	0.0232	0.0214
R1[a] [$I > 2\sigma(I)$]	0.0364	0.0362	0.0513	0.0274	0.0378
wR2[b] (all data)	0.0994	0.1164	0.1712	0.0728	0.0999
GOF	1.052	1.092	0.953	1.065	1.047

[a] $R1 = \sum||F_o| - |F_c||/\sum|F_o|$. [b] $wR2 = \{[\sum w(F_o^2 - F_c^2)^2]/\sum[w(F_o^2)^2]\}^{1/2}$.

dx.doi.org/10.1021/ic5011902 | Inorg. Chem. 2014, 53, 8129−8135

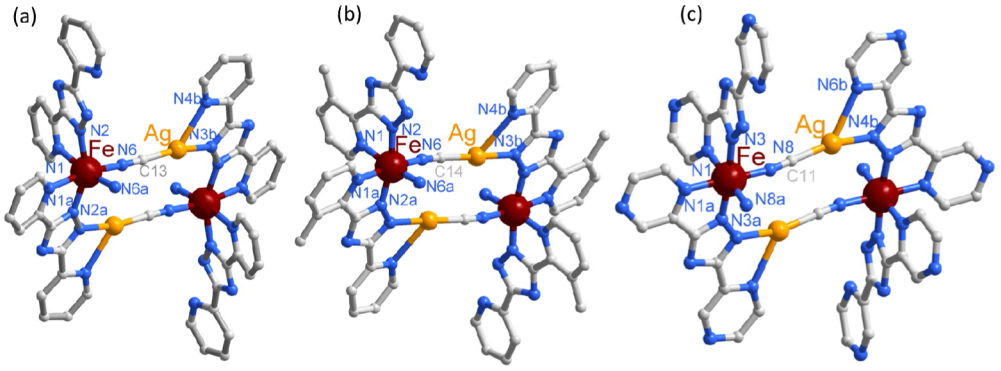

Figure 1. Coordination geometries of **1** (a), **2** (b), and **3** (c). Color code: Fe, red; Ag, orange; N, blue; C, gray.

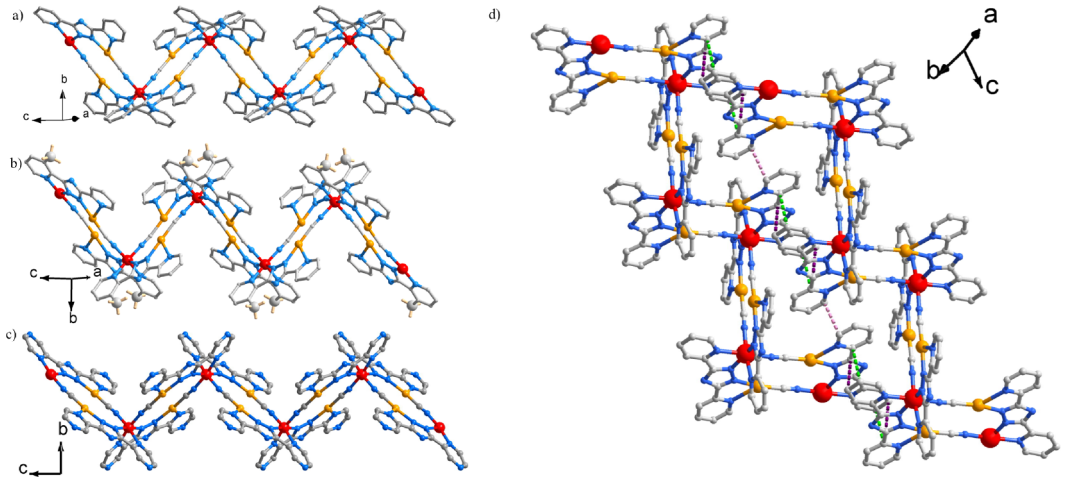

Figure 2. Side views of a 1D chain of **1** (a), **2** (b), and **3** (c). Packing diagram of 1D chains of **1** with the interchain $\pi\cdots\pi$ interactions (d). Hydrogen atoms were deleted for clarity.

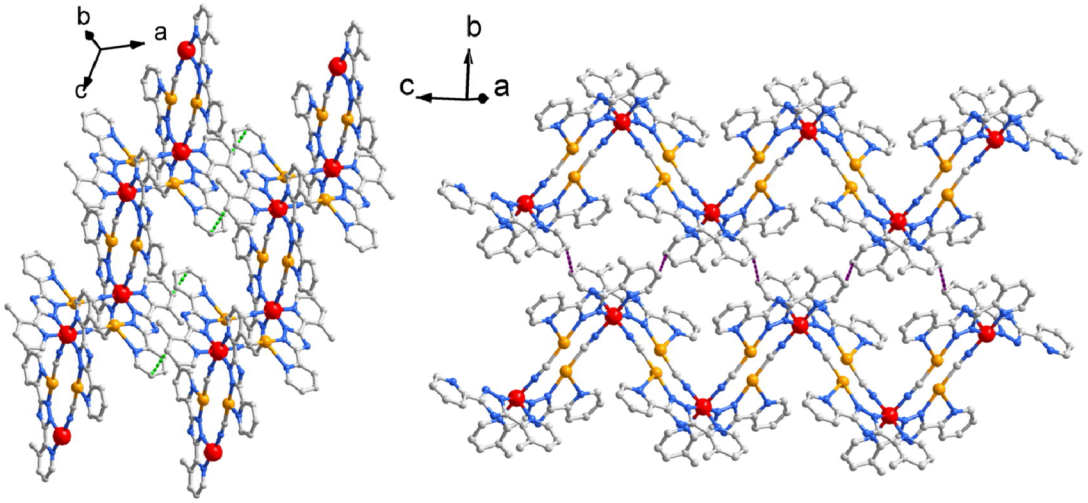

Figure 3. Packing diagram of 1D chains of **2** at 150 K with the interchain $\pi\cdots\pi$ interactions. Hydrogen atoms and solvent molecules were deleted for clarity.

weaker cumulative formation constant (log K_2 = 21.1 for $[Ag(CN)_2]^-$ and log K_2 = 38.3 for $[Au(CN)_2]^-$).[10]

Crystal Structures. Complexes **1**−**3** crystallize in the monoclinic space group (Table 1) without crystallographic phase transition at 298 and 150 K. There is no lattice solvent molecule in **1** and **3**, while disordered ethanol in **2** is removed by *SQUEEZE*.[9b] The asymmetric units of **1**−**3** consist of one substituted bpt^- ligand connecting one Fe^{II} ion (half-occupied) and one in situ generated AgCN species in a cis bridging mode (Figure 1). Each Fe^{II} ion is octahedrally surrounded by four nitrogen atoms from two substituted bpt^- ligands and two nitrogen atoms from two AgCN species in a cis arrangement. Each silver ion is bonded to a carbon atom from the cyanide ion and two nitrogen atoms from the bpt^- ligand in a distorted

dx.doi.org/10.1021/ic5011902 | *Inorg. Chem.* 2014, 53, 8129−8135

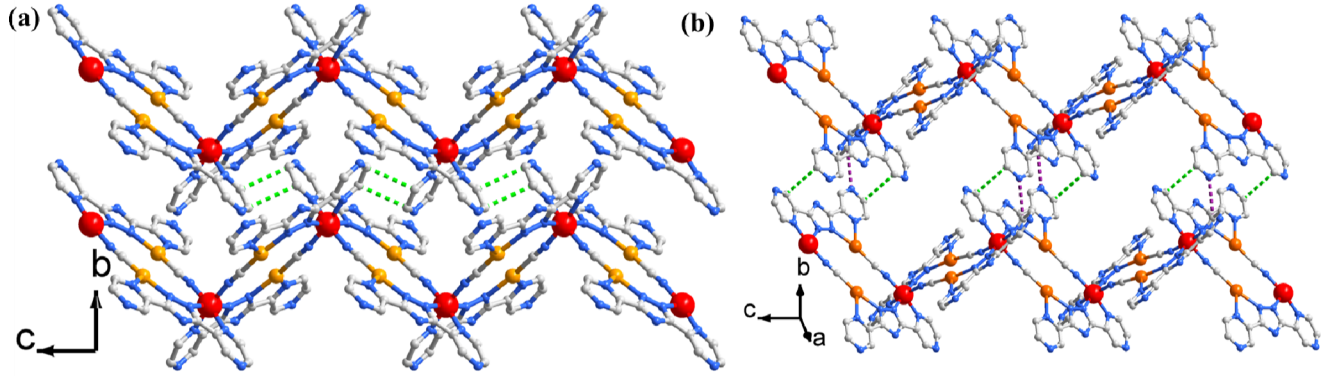

Figure 4. Packing diagram of 1D chains of **3** at 150 K with the interchain $\pi\cdots\pi$ interactions. Hydrogen atoms were deleted for clarity.

trigonal geometry. A rhombus $\{Fe_2Ag_2\}$ unit is generated by inversion, as shown in Figure 1. Then it forms a 1D zigzag chain, which reflects the cis arrangement of two bpt^- and AgCN ligands in the iron coordination sphere, as shown in Figure 2. A three-dimensional (3D) supramolecular structure is further formed by interchain $\pi\cdots\pi$ interactions (Figures 2−4). It is worth noting that weak Ag···N interactions (2.825 Å at 298 K) occur between the neighboring chains present in complex **3** (Figure 5).

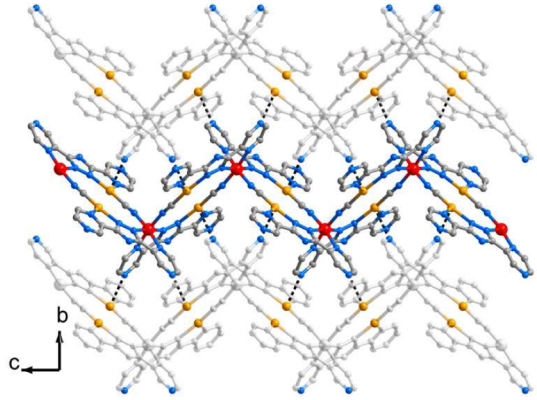

Figure 5. Intermolecular Ag···N interactions in **3** at 150 K. Hydrogen atoms were deleted for clarity.

Further investigation is performed to study the magneto-structural relationships in detail below. As shown in Table 2, their relevant bond distances and angles are presented. The average Fe−N distances of **1**−**3** at ambient temperature are in line with that of HS Fe^{II} complexes. Meanwhile, the average Fe−N distances of **2** and **3** at 150 K are 1.970 and 1.962 Å, respectively, which are consistent with LS Fe^{II} ions. The Σ values decrease from 71.38° and 79.92° at 298 K to 42.46° and 52.79° at 150 K in **2** and **3**, respectively, in accordance with a more regular octahedral geometry in the LS state.[3b,11] It is also in line with the spin-state assignments derived from average Fe−N distance analysis.

The 3D supramolecular structure of **1** organized by an offset face-to-face $\pi\cdots\pi$ interaction between triazole and pyridine groups (C3···C7 = 3.393 Å) and two offset face-to-face $\pi\cdots\pi$ interactions between two pyridine groups (C2···C8 = 3.442 Å and C12···C12 = 3.281 Å; in Table 3). In contrast, only one kind of C···C intermolecular contact in **2** at 298 K is shorter than 3.6 Å, which is the sum of the van der Waals distances for the carbon atom. When the temperature is decreased, the supramolecular structure of **2** is tightly stacked by offset face-to-face $\pi\cdots\pi$ interactions between 3-methylpyridine and pyridine groups (C3···C11 = 3.392 Å) and an offset face-to-face $\pi\cdots\pi$ interaction between two 3-methylpyridine groups (C2···C2 = 3.292 Å), as shown in Figure 3. In the case of **3** at 298 K, the supramolecular structure is packed by offset face-to-face $\pi\cdots\pi$ interactions (C1···C2 = 3.321 Å and C3···C9 = 3.377 Å) and an edge-to-face $\pi\cdots\pi$ interaction (C1···N7 = 3.246 Å) between two

Table 2. Selected Bond Lengths (Å) and Angles (deg) of 1−3 at 298 and 150 K

				Compound **1**				
	Fe1−N_{trz}	Fe1−N_{py}	Fe1−N_{AGCN}	Fe1−N_{av}	∑Fe1	Ag1−N3	Ag1−N4	Ag1−C13
298 K	2.151	2.281	2.116	2.183	77.62	2.143	2.601	2.045
				Compound **2**				
	Fe1−N_{trz}	Fe1−N_{mepy}	Fe1−N_{AGCN}	Fe1−N_{av}	∑Fe1	Ag1−N3	Ag1−N4	Ag1−C14
150 K	1.962	2.024	1.925	1.970	42.46	2.152	2.695	2.058
298 K	2.108	2.236	2.077	2.141	71.38	2.145	2.671	2.072
change	0.146	0.222	0.158	0.171	28.93	−0.007	−0.024	0.014
				Compound **3**				
	Fe1−N_{trz}	Fe1−N_{pz}	Fe1−N_{AGCN}	Fe1−N_{av}	∑Fe1	Ag1−N4	Ag1−N6	Ag1−C11	Ag1−N2
150 K	1.966	1.969	1.952	1.962	52.79	2.217	2.598	2.082	2.751
298 K	2.150	2.221	2.090	2.182	79.92	2.207	2.604	2.060	2.825
change	0.184	0.252	0.138	0.220	27.13	−0.010	0.006	−0.022	0.074

[a] Fe1−N_{av} is the average Fe−N distance.

dx.doi.org/10.1021/ic5011902 | Inorg. Chem. 2014, 53, 8129−8135

Table 3. Supramolecular $\pi\cdots\pi$ Interactions (Å) for 1−3[a]

1	298	C(3)···C(7a) 3.393	C(2)···C(8a) 3.442	C(12)···C(12b) 3.281
2	150	C(3)···C(11c) 3.392		C(2)···C(2d) 3.292
	298	C(3)···C(11c) 3.503		C(2)···C(2d) 3.653
3	150	C1···N(7e) 3.142	C(3)···C(9f) 3.452	C(1)···C(2g) 3.136
	298	C1···N(7e) 3.246	C(3)···C(9f) 3.377	C(1)···C(2g) 3.321

[a]Symmetry codes: a, 0.5 − *x*, 1.5 − *y*, 1 − *z*; b, *x*, −*y*, *z* − $^1/_2$; c, 0.5 − *x*, 0.5 − *y*, 2 − *z*; d, 1 − *x*, 1 − *y*, 3 − *z*; e, −1 − *x*, *y*, −1.5 − *z*; f, −*x* + 1, −*y* + 1, −*z*; g, −*x*, 1 − *y*, −1 − *z*.

pyrazine groups. At 150 K, these intermolecular contacts of C1···C2, C3···C9, and C1···N7 become 3.136, 3.452, and 3.142 Å, respectively. In addition, the Ag1···N2 interaction (2.825 Å at 298 K) is present in complex **3**, which decreases to 2.750 Å at 150 K.

Magnetic Properties. The magnetic properties were studied on polycrystalline samples of **1**−**3** (Figure 6). In the case of **1**, the $\chi_M T$ value gradually decreases from 3.71 cm^3 K mol^{-1} at 298 K to 3.56 cm^3 K mol^{-1} at 50 K, indicative of a magnetically anisotropic HS Fe^{II} ion (Figure 6a), and then decreases suddenly below 50 K, which should be the zero-field splitting of a HS Fe^{II} ion.

In the case of **2**, the $\chi_M T$ value is 3.18 cm^3 K mol^{-1} at 300 K, suggesting a HS Fe^{II} ion at ambient temperature (Figure 6b). It decreases gradually when cooling to 240 K, drops more steeply to 0.32 cm^3 K mol^{-1} at 140 K, and then decreases gradually to 0.03 cm^3 K mol^{-1} at 2 K, which is close to the value expected for a diamagnetic LS Fe^{II} ion. Therefore, it undergoes gradual and complete SCO behavior. Two subsequent cooling−heating cycles suggest the presence of a stable thermal hysteresis loop with 3 K width ($T_{1/2}\downarrow$ = 232 K and $T_{1/2}\uparrow$ = 235 K). The light-induced excited-spin-state trapping (LIESST) effect[12] of **2** was explored by applying blue light (473 nm) to irradiate a sample to saturation at 5 K for 6 h. The maximum $\chi_M T$ value at 20 K (1.48 cm^3 K mol^{-1}) indicated that a photoexcited population of approximately 40% HS Fe^{II} ion was achieved.

For complex **3** (Figure 6c), the $\chi_M T$ value drops slowly from 3.36 cm^3 K mol^{-1} at 330 K to 3.04 cm^3 K mol^{-1} at 289 K and then drops steeply to 0.87 cm^3 K mol^{-1} at 284 K, which indicates an abrupt SCO with $T_{1/2}\downarrow$ = 286 K. Below 284 K, the $\chi_M T$ value continuously decreases to 0.37 cm^3 K mol^{-1} at 5 K. The subsequent heating mode provides evidence for a 6 K hysteresis loop with $T_{1/2}\uparrow$ = 292 K. No LIESST effect was observed in **3**.

The SCO behaviors in **2** and **3** were further corroborated by DSC experiments (Figure 7). For complex **2**, it revealed an exothermic peak at $T_{1/2}\downarrow$ = 231 K and an endothermic peak at $T_{1/2}\uparrow$ = 234 K, delineating a hysteresis loop of 3 K. Meanwhile, it revealed a typical anomaly at $T_{1/2}\downarrow$ = 283 K and $T_{1/2}\uparrow$ = 289 K for **3**, delineating a hysteresis loop of 6 K. The variations of enthalpy (ΔH) and entropy (ΔS) are ΔH = 7.53 kJ mol^{-1} and ΔS = 32.70 J K^{-1} mol^{-1} for **2** and ΔH = 14.09 kJ mol^{-1} and ΔS = 48.72 J K^{-1} mol^{-1} for **3**, which are within the experimental range for Fe^{II} SCO systems.[12a,13]

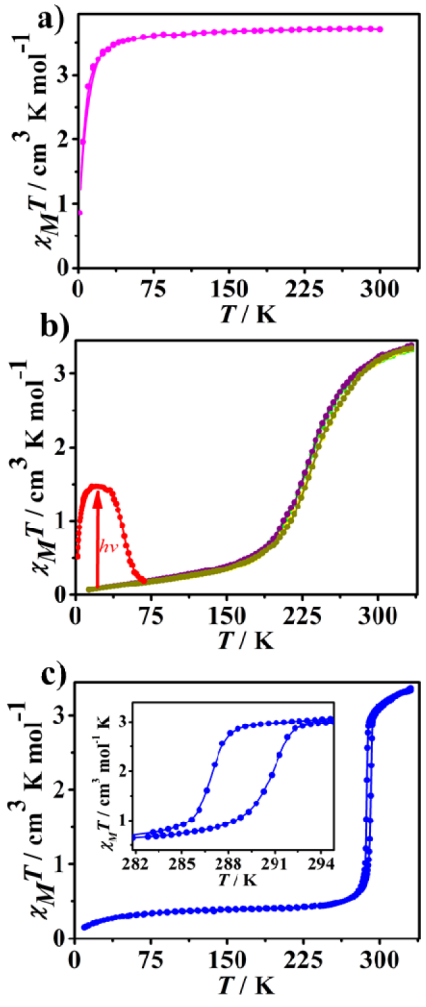

Figure 6. Temperature-dependent $\chi_M T$ plot for **1** (a) (magenta), **2** [two cycles before (purple, dark yellow, green, and yellow) and after (red) irradiation], and **3** (blue).

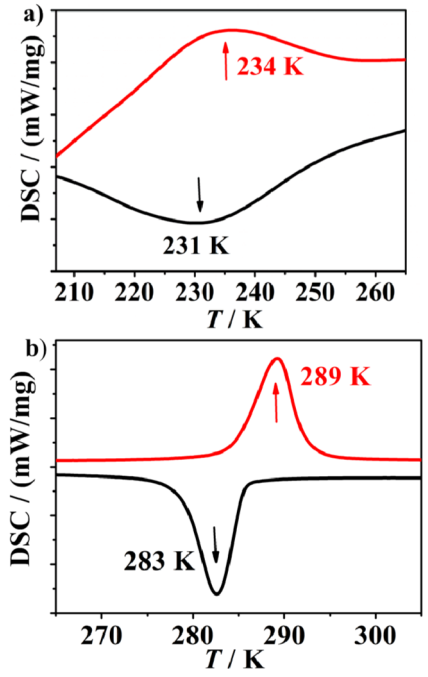

Figure 7. DSC curves of **2** (a) and **3** (b). The heating and cooling modes are in red and black with a rate of 10 K min^{-1}, respectively.

dx.doi.org/10.1021/ic5011902 | Inorg. Chem. 2014, 53, 8129−8135

To elucidate the degree of cooperativeness inherent in **2** and **3**, the excess heat capacity ΔC_p versus T curve was evaluated by the domain model developed by Sorai and Seki[14] in terms of the number of molecules per domain n.

$$\Delta C_p = \frac{n(\Delta H)^2}{RT^2} \frac{\exp\left[\frac{n\Delta H}{R}\left(\frac{1}{T} - \frac{1}{T_{1/2}}\right)\right]}{\left\{1 + \exp\left[\frac{n\Delta H}{R}\left(\frac{1}{T} - \frac{1}{T_{1/2}}\right)\right]\right\}^2}$$

As n is increased, the cooperativeness of SCO becomes stronger and the heat capacity peak becomes sharper. The values of n were about 1.5 for gradual SCO $[Fe(2\text{-pic})_3]Cl_2 \cdot CH_3OH$ and 95 for abrupt SCO $[Fe(phen)_2(NCS)_2]$, respectively.[15] As shown in Figure 8, the experimental ΔC_p data derived from DSC experiments were very satisfactorily fit to the equation while leaving all parameters free. The value of n = 10.8 (Table 4) in **2** suggests somewhat weak cooperativity, which is consistent with the gradual SCO behavior and broad heat capacity peak. Meanwhile, the larger value of n = 42.1 in **3** indicates stronger cooperativity, which is in line with the abrupt SCO behavior and sharp heat capacity peak.

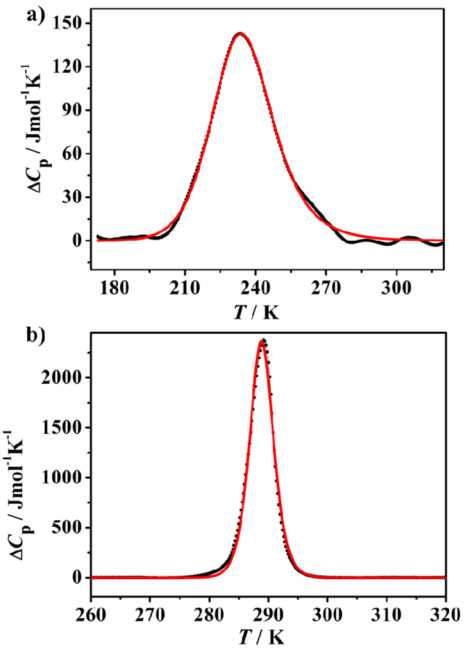

Figure 8. Excess heat capacity for **2** (a) and **3** (b) upon warming. They are fitted to the domain model (red line).

Table 4. Fitted Values ($T_{1/2}$ and n) to the Domain Model for 2 and 3

complex	cooperativity (n)	$T_{1/2}$ (K)
2	10.8	235
3	42.1	288

Discussion. Because the substituent effects and intermolecular interactions play important roles in the magnetic behaviors,[3,4] deep insight into the magnetostructural relationship is explored on the present $[Fe^{II}(L)_2(AgCN)_2]$ system. At first glance, by considering the electronic substituent effects, the methyl substituent of the Mebpt$^-$ ligand and the nitrogen atom of the bpzt$^-$ ligand may serve to increase the electron density and back-donation in the pyridine rings, respectively,[4d,8,16] and then result in enhancement of the ligand-field strength, which is estimated to be responsible for the improved magnetic behavior in **2** and **3**. A similar situation of the substituent effect in the Co^{II} system was reported.[17] Second, the $\pi\cdots\pi$-stacking interaction also plays an important role in the SCO properties. As shown in Table 3, there are three and two pairs of offset face-to-face $\pi\cdots\pi$-stacking interactions in **1** and **2**, respectively. Meanwhile, there are two pairs of offset face-to-face $\pi\cdots\pi$-stacking interactions and one pair of edge-to-face $\pi\cdots\pi$-stacking interactions in **3**. The presence of different magnetic behaviors in these compounds can be explained to some extent by the existence of $\pi\cdots\pi$-stacking intermolecular interactions.[3,18] Finally, the interchain Ag···N distance in complex **3** is 2.750 Å at 150 K (2.824 Å at 298 K), indicating the relatively weak coordination bonds. In other words, a pseudo-2D structure is formed through the interchain Ag···N interaction. Then the difference in dimensionality can be the reason for the hysteresis loop of **3** being wider than that of **2**.[19] Thus, the factors of the electronic substituent effect, the $\pi\cdots\pi$ interactions, and the weak Ag···N coordination bond interactions work together and finally result in an abrupt SCO with hysteresis near room temperature for complex **3**. In contrast to **2**, the LIESST effect was not observed in **3**, which may be due to the stronger ligand-field strength in **3** because the stronger this factor, the shorter the lifetime of the LIESST state.[20]

CONCLUSION

In summary, we have synthesized three 1D hetereobimetallic coordination polymers $[Fe^{II}(L)_2(AgCN)_2]$ with in situ generated AgCN species and substituent bpt$^-$ ligands. Their magnetic behaviors can be dramatically affected by the electronic substituent effect and intermolecular interactions: **1** displays paramagnetic behavior, while **2** and **3** undergo gradual and abrupt SCO behaviors, respectively. Importantly, the electronic substituent effect, $\pi\cdots\pi$ interactions, and weak Ag···N coordination bond interactions in **3** work together and provide relatively high cooperativeness with an estimated 42.1 molecules per domain, which leads to an abrupt SCO behavior with a thermal hysteresis loop of 6 K near room temperature. Further studies on the fabrication of new materials presenting abrupt and hysteretic SCO behaviors centered near room temperature are currently underway.

ASSOCIATED CONTENT

Supporting Information

X-ray crystallographic data in CIF format, PXRD patterns for **1**−**3**, and UV−vis spectra of complex **2** and the MebptH ligand. This material is available free of charge via the Internet at http://pubs.acs.org.

AUTHOR INFORMATION

Corresponding Authors

*E-mail: nizhp@mail.sysu.edu.cn.
*E-mail: tongml@mail.sysu.edu.cn.

Notes

The authors declare no competing financial interest.

ACKNOWLEDGMENTS

This work was supported by the "973 Project" (Grants 2012CB821704 and 2014CB845600), the NSFC (Grants

91122032, 21201182, 21373279, and 21121061), and the Program for Changjiang Scholars and Innovative Research Team in University of China (Grant IRT1298).

REFERENCES

(1) (a) Gütlich, P., Goodwin, H. A., Eds. Spin Crossover in Transition Metal Compounds I, II and III. *Topics in Current Chemistry*; Springer-Verlag: Berlin, 2004; Vols. *233*−*235*. (b) Halcrow, M. A. *Spin-crossover materials: properties and applications*; John Wiley & Sons, Ltd.: New York, 2013.
(2) (a) Kahn, O.; Martinez, C. J. *Science* **1998**, *279*, 44−48. (b) Létard, J.-F.; Guionneau, P.; Goux-Capes, L. *Top. Curr. Chem.* **2004**, *235*, 221−249.
(3) (a) Murray, K. S.; Kepert, C. J. *Top. Curr. Chem.* **2004**, *233*, 195−228. (b) Halcrow, M. A. *Chem. Soc. Rev.* **2011**, *40*, 4119−4142.
(4) (a) Kitchen, J. A.; Brooker, S. *Coord. Chem. Rev.* **2008**, *252*, 2072−2092. (b) Bao, X.; Liu, J.-L; Leng, J.-D.; Lin, Z.-J.; Tong, M.-L.; Nihei, M.; Oshio, H. *Chem.—Eur. J.* **2010**, *16*, 7973−7978. (c) Bao, X.; Guo, P.-H.; Liu, J.-L; Leng, J.-D.; Tong, M.-L. *Chem.—Eur. J.* **2011**, *17*, 2335−2339. (d) Bao, X.; Guo, P.-H.; Liu, W.; Tucek, J.; Zhang, W. X.; Leng, J. D.; Chen, X. M.; Gural'skiy, I.; Salmon, L.; Bousseksou, A.; Tong, M.-L. *Chem. Sci.* **2012**, *3*, 1629−1633. (e) Zhang, X. T.; Sun, D.; Li, B.; Fan, L. M.; Li, B.; Wei, P. H. *Cryst. Growth Des.* **2012**, *12*, 3845−3848. (f) Lin, J.-B.; Xue, W.; Wang, B.-Y.; Tao, J.; Zhang, W.-X.; Zhang, J.-P.; Chen, X.-M. *Inorg. Chem.* **2012**, *51*, 9423−9430. (g) Liu, W.; Bao, X.; Mao, L.-L.; Tucek, J.; Zboril, R.; Liu, J.-L.; Guo, F.-S.; Ni, Z.-P.; Tong, M.-L. *Chem. Commun.* **2014**, *50*, 4059−4061.
(5) Bao, X.; Leng, J.-D.; Meng, Z.-S.; Lin, Z.-J.; Tong, M.-L.; Nihei, M.; Oshio, H. *Chem.—Eur. J.* **2010**, *16*, 6169−6174.
(6) (a) Schneider, C. J.; Cashion, J. D.; Moubaraki, B.; Neville, S. M.; Batten, S. R.; Turner, D. R.; Murray, K. S. *Polyhedron* **2007**, *26*, 1764−1772. (b) Schneider, C. J.; Cashion, J. D.; Chilton, N. F.; Etrillard, C.; Fuentealba, M.; Howard, J. A. K.; Létard, J.-F.; Milsmann, C.; Moubaraki, B.; Sparkes, H. A.; Batten, S. R.; Murray, K. S. *Eur. J. Inorg. Chem.* **2013**, 850−864.
(7) Yan, Z.; Ni, Z.-P.; Guo, F.-S.; Li, J.-Y.; Chen, Y.-C.; Liu, J.-L.; Lin, W.-Q.; Aravena, D.; Ruiz, E.; Tong, M.-L. *Inorg. Chem.* **2014**, *53*, 201−208.
(8) Goodgame, D. M. L.; Goodgame, M.; Hitchman, M. A.; Weeks, M. J. *Inorg. Chem.* **1966**, *5*, 635−638.
(9) (a) Sheldrick, G. M. *SHELXTL97, program for crystal structure refinement*; University of Göttingen: Göttingen, Germany, 1997. (b) Spek, A. L. *J. Appl. Crystallogr.* **2003**, *36*, 7−13. (c) Spek, A. L. *Acta Crystallogr.* **2009**, *D65*, 148−155.
(10) Speight, J. G., Ed. *Lange's Handbook of Chemistry 70th Anniversary*; McGraw-Hill Publishers: New York, 2005.
(11) (a) Guionneau, P.; Marchivie, M.; Bravic, G.; Létard, J.-F.; Chasseau, D. *J. Mater. Chem.* **2002**, *12*, 2546−2551. (b) Guionneau, P.; Marchivie, M.; Bravic, G.; Létard, J.-F.; Chasseau, D. *Top. Curr. Chem.* **2004**, *234*, 97−128.
(12) (a) Guionneau, P.; Hauser, A.; Spiering, H. *Angew. Chem., Int. Ed.* **1994**, *33*, 2024−2054. (b) Hauser, A. *Top. Curr. Chem.* **2004**, *234*, 155−198.
(13) Gütlich, P.; Garcia, Y.; Goodwin, H. A. *Chem. Soc. Rev.* **2000**, *29*, 419−427.
(14) (a) Sorai, M.; Seki, S. *J. Phys. Chem. Solids* **1974**, *35*, 555−570. (b) Sorai, M. *Top. Curr. Chem.* **2004**, *235*, 153−170. (c) Sorai, M.; Nakano, M.; Miyazaki, Y. *Chem. Rev.* **2006**, *106*, 976−1031.
(15) Nakamoto, T.; Tan, Z. C.; Sorai, M. *Inorg. Chem.* **2001**, *40*, 3805−3809.
(16) Lever, A. B. P.; Lewis, J.; Nyholm, R. S. *J. Chem. Soc.* **1964**, 4761−4768.
(17) Cowan, M. G.; Olguín, J.; Narayanaswamy, S.; Tallon, J. L.; Brooker, S. *J. Am. Chem. Soc.* **2012**, *134*, 2892−2894.
(18) González-Prieto, R.; Fleury, B.; Schramm, F.; Zoppellaro, G.; Chandrasekar, R.; Fuhr, O.; Lebedkin, S.; Kappes, M.; Ruben, M. *Dalton Trans.* **2011**, *40*, 7564−7570.
(19) Niel, V.; Martínez-Agudo, J. M.; Muñoz, M. C.; Gaspar, A. B.; Real, J. A. *Inorg. Chem.* **2001**, *40*, 3838−3839.
(20) Gütlich, P.; Garcia, Y.; Woike, T. *Coord. Chem. Rev.* **2001**, *219*−*221*, 839−879.